Spectral Shape Analysis of Human Torsos: Application to the Evaluation of Scoliosis Surgery Outcome

Ola Ahmad, Herve Lombaert, Stefan Parent, Hubert Labelle, and Farida Cheriet

***Abstract*—This paper aims at evaluating the effect of spinal surgery on the torso shape appearance of adolescent patients. Current methods that assess the surgical outcome on the trunk shape are limited to its global asymmetry or rely on unreliable manual measurements. We introduce a novel framework to evaluate pre- to postoperative local asymmetry changes using a spectral representation of the torso shape, more specifically, the Laplacian spectrum (eigenvalues and eigenvectors) of a graph. We conduct a statistical analysis on the eigenvalues to efficiently select the spectral space and determine the significant components between preop and postop groups. On the selected eigenvectors, we propose a local analysis based on the concept of Euler characteristic to detect their local maxima and minima, which are then used to compute local left–right (L–R) asymmetries of torso shape. On 49 patients with a thoracic spinal deformity, the method captures significant pre- to postoperative changes of asymmetry at the waist, shoulder blades, shoulders, and breasts. We have evaluated average correction rates for L–R asymmetry of the waist height (67%), shoulder-blade height (64%) and depth (67%), lateral offset between shoulder and neck (61%), and breast height (52%). Spectral torso shape analysis provides a novel approach to quantify the surgical correction of the scoliotic trunk from local shape asymmetry. The proposed method could help the surgeon to understand the impact of different spinal surgery strategies on the postoperative appearance and choose the one that should provide better patient's satisfaction.**

***Index Terms*—3D torso model, graph Laplacian, scoliosis, spectral representation, statistical shape analysis, surgical outcome assessment, topology.**

Manuscript received February 14, 2017; revised September 2, 2017 and September 26, 2017; accepted September 30, 2017. Date of publication October 9, 2017; date of current version August 31, 2018. This work was supported by the Canadian Institutes of Health Research Grant MPO 125875. *(Corresponding author: Ola Ahmad.)*

O. Ahmad and F. Cheriet are with the Polytechnique Montréal, Montréal, QC H3T 1J4, Canada, and also with the CHU Sainte-Justine Paediatric Hospital, Montréal, QC H3T 1C5, Canada (e-mail: olasahmad@gmail.com; farida.cheriet@polymtl.ca).

H. Lombaert is with the École de Téchnologie Supérieure, Montréal, QC H3C 1K3, Canada, and also with the INRIA Sophia-Antipolis, Valbonne 06902, France (e-mail: herve.lombaert@gmail.com).

S. Parent and H. Labelle are with the University of Montreal, Montréal, QC H3T 1J4, Canada, and also with the CHU Sainte-Justine Paediatric Hospital, Montréal, QC H3T 1C5, Canada (e-mail: stefan.parent@umontreal.ca; hubert.labelle@recherche-ste-justine.qc.ca).

Digital Object Identifier 10.1109/JBHI.2017.2759804

I. Introduction

ADOLESCENT idiopathic scoliosis (AIS) is a three-dimensional deformation leading to a lateral curvature of the spine associated with vertebral and rib cage rotation [1], [2]. This deformation generates visible asymmetries on the torso shape (see Fig. 1), which in turn affect the external appearance of the trunk [3]. While this pathology is commonly diagnosed in childhood and adolescents aged 10–18 years old, it can progress rapidly during the adolescent growth spurt to the point of requiring spinal surgery [4]. Indeed, severe scoliosis may, in addition to trunk shape deformations, lead to functional problems such as cardiac and pulmonary dysfunction, cause common backaches, and decrease the physical capacity of patients [5], [6]. Surgical treatment in the case of sever scoliosis is therefore highly recommended to correct the spinal curvature and stop its progression, thereby improving the quality of life of adolescent patients.

The outcome of scoliosis surgery is usually evaluated by examining the global balance of the torso. This is based on radiographic measurements, mainly Cobb angles [7] that quantify the spinal curvatures. The Cobb angle evaluates accurately the changes in the curve amplitudes observed from frontal and lateral radiographs [8]. However, these measurements cannot assess the changes in the external asymmetries or the appearance of torso, which are the primary indicators of a patient's satisfaction with the surgery [9]. Some studies invoke questionnaires for patients with medical [9] and non-medical [10], [11] raters to include an evaluation of the external shape. But such evaluations are often qualitative and affected by a subjective judgment. For these reasons, a variety of approaches were developed in order to provide quantitative measurements of the torso asymmetry that allow a more reliable assessment of the scoliosis surgery outcome.

The most popular clinical assessment tool used to quantify torso shape asymmetry is the manual scoliometer [12]. This tool was developed mainly to measure the rib hump—an asymmetrical thoracic prominence on the back induced by ribcage deformation—while the patient is on forward-bending (see right image in Fig. 5). Recently, the scoliometer technique was used in [13] to assess the effectiveness of scoliosis surgery to reduce the posterior rib and lumbar prominences. However, the uncertainties related to the patient's posture and the manual method lead to unreliable and irreproducible shape

Fig. 1. Four samples of adolescent patients with AIS. The scoliotic deformations on torso shapes include global misalignments and axial rotations as well as local asymmetries in shoulders, waist, scapula, hips and thoracic prominence.

measurements. Optical techniques that provide a mapping of the back surface have been used as a viable alternative to scoliometer measurements. Each of these techniques extracts, manually or semi-automatically, a set of anatomic landmarks from the back surface to quantify the asymmetries in terms of distances and angles. A survey of all these techniques is given in [14]. In contrast, cross-sectional based methods [15], [16] benefit from measuring the whole torso shape, which is usually in the form of a 3D triangulated mesh. The surface is partitioned into uniform 2D cross-sections and functional asymmetry indices are then computed. For example, bend, tilt and twist asymmetries are defined in [15]; back surface rotation, trunk rotation and trunk lateral shift are the asymmetry indices defined in [16]. This later method was recently used to evaluate the outcome of spinal surgeries on torso shape [17]. The underlying functional asymmetries are, however, global in their nature and cannot be used to evaluate local shape changes, as for instance, local corrections of torso deformity after surgery.

Various shape representations have been proposed to study local shape changes across populations of shape meshes. For instance, spherical-based shape representations [18], [19], Surface parametrization using Fourier descriptors [20], and medial representations [21], [22]. These methods generally rely on one or more important pre-processing tasks like re-meshing, registration, or one-to-one correspondence. In contrast, spectral methods [23], [24] offer isometric-invariant shape descriptors that characterize the intrinsic geometry of the mesh, i.e., meshes with identical geodesics between vertices have identical spectral features. A recent comprehensive survey on the spectral approaches shows their power in many computer vision fields [25]. With minimal pre-processing—without registration or correspondence—spectral shape descriptors have been efficiently used to compare shapes [26]–[28]. In particular, a smooth representation of surface geometry (a manifold) is defined on a triangle mesh, where the eigenvalues of the Laplace-Beltrami (LB) operator are computed and defined as the shape-DNA [26]. This study demonstrated the robustness and efficiency of using the spectral shape-DNA to compare global changes of surfaces and solids. An extended work proposed to incorporate the spectral eigenfunctions analysis with shape-DNA to allow a local comparison between subcortical brain surfaces [27]. Although this work discussed several relevant topics relating to the LB spectrum, we focus here on its use for local shape analysis. The local analysis [27] exploits the topological structure of the smooth LB eigenfunctions. This topology is introduced by level sets, nodal curves and Morse-Smale complex [29], and is used to detect the thickness and size changes of caudate shapes.

Motivated by the previous spectral shape analysis approaches, we propose here a new method based on shape spectra to evaluate local asymmetry changes between pre- and post-operative torso shapes. In a previous study [30], we used a Laplacian operator of a graph model to compute the spectral representation of the trunk surface. This study was limited to demonstrating that the graph spectrum is able to find the optimal correspondence between torso shapes, thereby allowing point-wise longitudinal analysis in scoliosis progression assessment. In this paper, we propose to analyze torso asymmetry changes using the Laplacian spectrum, while local geometric features (maxima and minima) of the most relevant eigenvectors are computed from a connected component analysis of their upper- and lower-level sets. More specifically, we propose the well-known Euler Characteristic (EC) concept [31] to describe the topological structure of the spectral embedding space. The EC is a class of invariant homology groups that characterizes the topology of the space, in the sense of counting the connected components and the *n-dimensional* holes. To the best of our knowledge, the use of algebraic topology (EC and connected components analysis) of the graph Laplacian for local shape comparisons has not yet been exploited.

The rest of the paper is organized as follows. Section II describes the proposed framework for analyzing pre- to post-operative asymmetry changes in scoliotic torso shapes. Section III presents our experimental results on a dataset of AIS patients with a single type of thoracic spinal deformity (Lenke 1A curve type [32]). These results are discussed in Section IV, and a conclusion is provided in Section V.

II. Proposed Framework for Change Analysis of Scoliotic Torso Models

We begin with the spectral representation of torso shape models based on the graph Laplacian matrix (Section II-A). Inspired by the Laplace-Beltrami shape-DNA [27], we describe in the following two subsections (Sections II-B and II-C) how the Laplacian features are used to compare scoliotic torso shapes. Finally, we present our novel method for quantifying local asymmetries of torso models from the relevant spectral components (Section II-D).

A. Spectral Representation of Torso Shape

We consider a discrete representation of deformable torso, i.e., a triangular mesh (M). We therefore use the general graph Laplacian [23] to represent the spectral components of M.

The connected undirected graph $\mathcal{G} = \{\mathcal{V}, \mathcal{E}\}$ is defined by the set of vertices $v_i \in \mathcal{V}$, and the set of edges $e_{ij} \in \mathcal{E}$ connecting neighboring vertices (v_i, v_j) of M. We assume that this graph is weighted, that is a $V \times V$ (V the total number of vertices) weighted adjacency matrix W is defined by non-negative weights derived from a distance metric on graph edges. We use

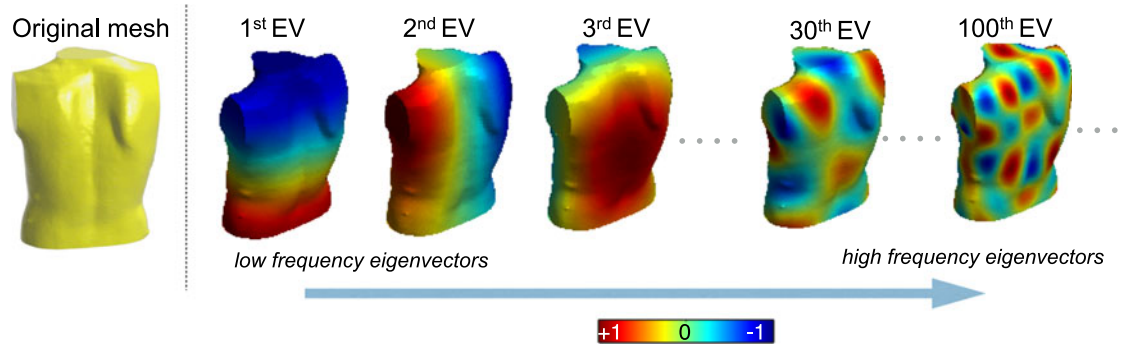

Fig. 2. Spectral representation of torso shape using the graph Laplacian. From left to right are the low to high frequency eigenvectors (EVs). *(The color bar indicates the eigenvectors amplitudes normalized to the range* $[-1, +1]$*.)*

the heat kernel to compute these weights:

$$W_{ij} = \begin{cases} e^{-\frac{\|\mathbf{x}_i - \mathbf{x}_j\|^2}{t}}, & \text{if } \exists\, e_{ij} \in \mathcal{E} \\ 0, & \text{otherwise.} \end{cases} \quad (1)$$

Where $t \in \mathbb{R}^+/\{0\}$ is, here, a scaling factor that controls the weight decay, $\mathbf{x}_i$ and $\mathbf{x}_j$ are the spatial coordinates of vertices i and j, respectively. For every node (or vertex), the spatial coordinate vector is given by $\mathbf{x} = (x, y, z)^T$. The heat kernel ensures smooth weights along the graph [33], and therefore allows to obtain more stable invariants than using the typical binary weights (i.e., $W_{ij} = 1$ if $e_{ij} \in \mathcal{E}$ and zero otherwise) or Euclidean distance.

The general Laplacian operator on the graph M was represented in [34] as the $V \times V$ matrix of the form

$$\mathcal{L} = D^{-1}(D - W) \quad (2)$$

where D is the diagonal degree matrix defined by the sum of weights as $D_{ii} = \sum_j W_{ij}$. The spectral decomposition of the Laplacian matrix $\mathcal{L} = \mathbf{\Phi}\Lambda\mathbf{\Phi}^{-1}$ is solved from the generalized eigenvalue problem, where $\Lambda = \text{diag}(\lambda_0, \lambda_1, ..., \lambda_V)$ is the diagonal matrix of the ordered eigenvalues, $(\lambda_0 \leqslant \lambda_1 \leqslant ...)$, and $\mathbf{\Phi} = (\Phi_0, \Phi_1, ..., \Phi_V)$ is the $V \times V$ matrix containing the associated eigenvectors, *eigenfunctions*, as column vectors. Since the graph is connected, the first eigenvalue $\lambda_0 = 0$—there is no boundary condition. The first eigenvector Φ_0 is thus a constant vector. The corresponding spectral embeddings have a multi-scale property. Fig. 2 shows how the spectral decomposition represents the harmonic behavior of the torso mesh surface. The lower eigenvectors correspond to the low frequency descriptors whereas higher eigenvectors capture geometric features at high frequencies.

B. Spectrum Normalization and Rearrangement

Torso shapes are generally of different sizes and their spectral eigenvalues are affected by size changes. Since the comparison between shapes needs to be independent of such size variations, their spectral features need to be normalized. As can be seen in Fig. 3, the eigenvalues of different torso shapes have approximately linear slops with respect to their orders. The differences between these slops are related to the variations of surface area

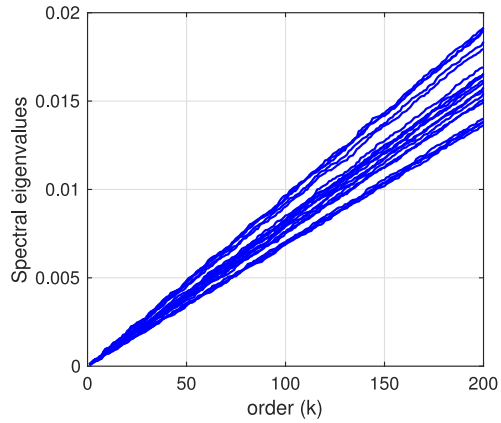

Fig. 3. Illustration of the first 200 spectral eigenvalues for a group of 20 postoperative AIS torso shapes. *Each profile corresponds to a torso shape sample.*

of the torso meshes, since the eigenvalues can asymptotically be given by $\lambda_k \propto c \times k/A(M)$ (c is a constant and $A(M)$ is the surface area of the mesh) as demonstrated on manifold shapes [26], [35]. Accordingly, we choose to normalize the eigenvalues using a linear regression function. On the other hand, the use of torso eigenvectors to quantify the local asymmetries requires us to ensure that the orders of the eigenvectors remain consistent with the ordered eigenvalues across samples. Usually, this is not true, since torso shape is not perfectly isometric. It is thus possible to get very close eigenvalues that may lead to changes in the orders and the orientation of the associated eigenvectors. Many state-of-the-art approaches have automatically addressed part of this problem using, for instance, heuristics [36], or similarity measures [37], [38]. These methods find the optimal permutation between eigenfunctions and correct the possible flipping of their signs. More recent studies have solved the problem entirely, i.e., order and rotation changes, by building joint matrices that transfer spectral eigenvectors between shapes [39]. We apply this later method to find the optimal arrangement between eigenvector pairs of different meshes. Here, we rearrange the eigenvectors of all scoliotic torso shapes with respect to an arbitrary shape selected from the postoperative population as a reference. In addition, we normalize all the eigenvectors to the range $[-1, +1]$ to facilitate their local analysis (Section II-D).

C. Statistical Analysis

1) Spectral Space Selection: Typically, the dimension of the spectral space is equal to the size of the input mesh, which is quite large (more than 20k vertices). In addition, not all these eigenvalues are relevant to the shape analysis. A selection of the relevant spectral components is thus required to ensure both computational efficiency and correct analysis. There are different ways to select the leading spectral components. Here, we employ a significance test between combinations of spectral eigenvalues across two groups (pre/post-operative) of torso shapes. More precisely, we search for significant differences between spectral representation pairs across the groups as a function of the spectral dimension. This can be achieved through a multivariate comparison. Usually in multivariate statistical testing problems, two well-known methods are considered: Hotelling's T^2–statistic or the maximum t–statistic of absolute differences [27], [40]. In this latter method, a permutation test is constructed to compute the exact significance level for each variable.

The maximum t-statistic is defined as follows

$$t_{\max} = \max_{1 \leqslant k \leqslant N} \frac{|\overline{\boldsymbol{v}}_{pre,k} - \overline{\boldsymbol{v}}_{post,k}|}{SD_k \cdot \sqrt{\frac{1}{n_{pre}} + \frac{1}{n_{post}}}} \tag{3}$$

where N defines the dimension variable of the spectral space, $\boldsymbol{v} = diag(\Lambda)$ is a column vector of the $N \times N$ eigenvalue matrix Λ, $\overline{\boldsymbol{v}}_{pre,k}$, $\overline{\boldsymbol{v}}_{post,k}$ are the average k–th eigenvalues of pre-operative (*pre*) and post-operative (*post*) scoliotic subjects, respectively, and SD_k is the pooled standard deviation of the k–th component over the two groups

$$SD_k = \sqrt{\frac{(n_{pre}-1)\sigma^2_{pre,k} + (n_{post}-1)\sigma^2_{post,k}}{n-2}} \tag{4}$$

with $\sigma^2_{pre,k}$ and $\sigma^2_{post,k}$ are the variances of the k–th component of each group, n_{pre} and n_{post} are their sample size, and $n = n_{pre} + n_{post}$ is the total number of observations. Please note that the outcome of the multivariate test is the p-value that indicates, for a significance level ($\alpha = 5\%$), the dimension of the spectral space, which consists of the first N leading eigenvalues. Also, we use the effect size, Cohen's d [41], to quantitatively compare the effect of the discrimination power of the spectral space between the groups independently of the sample size. Cohen's d is defined as the magnitude of the difference between the groups, divided by the standard deviation of each group, and it is commonly expressed in absolute values.

2) Detection of the Relevant Eigenvalues Reflecting Changes of Torso Asymmetries: The selected spectral space consists of at least one or more eigenvalues whose mean values have significantly changed between the two groups; they indicate a significant global change in torso asymmetry as a result of scoliosis surgery. A test statistic applied on the individual spectral components will determine the significant ones. Consequently, we investigate multiple hypotheses simultaneously on the N selected eigenvalues by invoking the false discovery rate (FDR) [42] to correct and adjust the p-values. At this stage, pairwise multiple comparisons based on the F-statistic are used to test pre- to post-operative shape differences by individual eigenvalues in the range $[1, N]$.

D. Identification and Quantification of Local Asymmetries

1) The Euler Characteristic (EC) and Connected Components Analysis: Although the spectral eigenvalues are the primary indicators of the significant changes in shape asymmetry, these changes are not directly interpretable, nor do they capture the *local* asymmetries. In contrast, the eigenvectors associated with the significantly changed eigenvalues provide a more refined and quantitative characterization of the local asymmetries. Referring to Fig. 2, the *k-th* eigenvector can have $m \leqslant k$ local features represented by local maxima and minima, which are surrounded by their connected components; these define a topological structure of the eigenvectors. Pairwise geometric distances between these local features on the left side of the torso and their counterparts on the right side quantify the degree of asymmetry in specific regions (e.g., shoulders, waists, breasts, etc.). The main challenge in detecting these local features is the unknown variations of their amplitude levels, which depend on the changes of the geometric deformations within and between shapes. We therefore propose to analyze the topology of the eigenvectors (associated with the relevant eigenvalues) through their level sets in order to detect all the underlying local features. Our topological method is based on the Euler characteristic (EC) of upper- (or lower-) level sets, where a level (u) is selected in the range $[-1, 1]$ to partition the mesh into local regions (or subdomains) located above and below u. This concept has been used in pattern recognition applications [43], [44], where the EC is derived from a probabilistic model of the image data. Here, we use the algebraic approach to compute the EC of subdomains obtained by the spectral embeddings. In addition, we adapt the concept of persistent connected components, contained in these subdomains, to detect the local geometric features of torso shape meshes.

Let M be a mesh with V vertices, E edges and F faces. The EC is then defined as

$$\chi_M = V - E + F \tag{5}$$

It is the alternating sum of the graph elements in each dimension: the vertices are of dimension 0 with the sign (+), the edges are of dimension 1 with the sign ($-$), and the faces are of dimension 2 with the sign (+). The same definition holds on partitions (or subsets) of M.

We define an upper-level set S_u of the mesh M as the subset of vertices and edges in which an eigenvector (ϕ) exceeds a threshold value u, such that

$$S_u = \{\mathbf{x} \in M,\, \phi(\mathbf{x}) \geqslant u\} \tag{6}$$

where $u \in [-1, 1]$. The upper-level sets at relatively high thresholds, i.e., near the upper bound of the range $[-1, 1]$, only consist of connected components including their local maxima, and the EC gives the number of these components. In the same context, the lower-level sets (i.e., $\{\mathbf{x} \in M, \phi(\mathbf{x}) \leqslant u\}$), or equivalently the upper-level sets of $-\phi$, include the local minima. We thus need to focus on relatively high (in the absolute sense) threshold

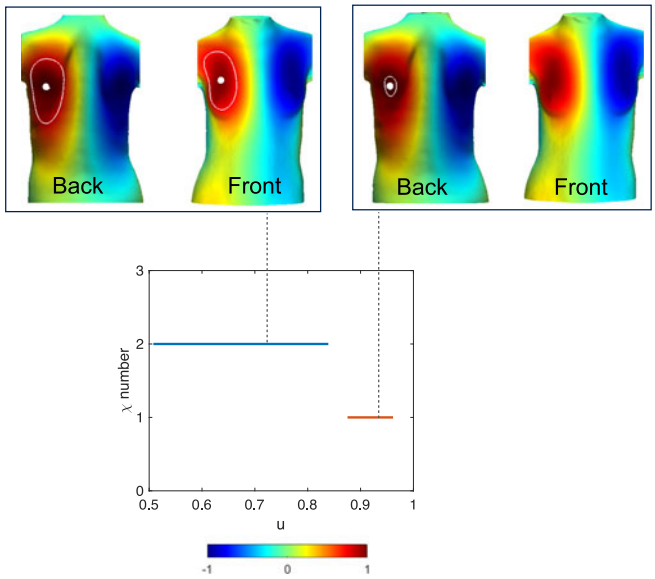

Fig. 4. The persistence for the EC of the connected components. Top row: *9-th* eigenvector of a post-operative torso of a female patient; from left to right, the figures show the upper-level sets (bounded by the white color) computed at $u = 0.73$ and $u = 0.95$, respectively; the white points are their local maxima. Bottom row: A bar diagram showing the persistence of the number of connected components over the range levels $[0.5, 1]$.

values, e.g., $u \in [0.5, 1]$, to detect these local features. However, when moving u from 0.5 to 1, the topology of S_u may change, i.e., some components may merge, disappear, or new ones may appear. Similarly, the EC number may change with respect to u. The persistence of EC indicates the life-time of the components and their significance (i.e., noise or features). For example, Fig. 4 shows the topological change of the *9-th* eigenvector, of a post-operative torso, as well as the persistence of the EC number—any other eigenvector can be used. In this figure, it can be seen (at bottom row) that $\chi = 2$ components rank a maximum persistence, starting at the level $u_1 = 0.5$ and ending at $u_2 = 0.87$. These components, as shown on the left of the top row, are located on the left-side shoulder blade and the left-side breast of the female torso. However, for $u > u_2$, one can notice, on the right of the top row of Fig. 4, that only the local maximum on the back side was detected at such high-level value whereas the connected component on the front disappeared. In this example, $\chi = 1$ ranks minimal persistence in the range $]0.87, 0.97]$, so any level in the range $[0.5, 0.87]$ can be selected to find all the local maxima of the *9-th* eigenvector. Finding the persistent connected components corresponding to the maximum persistence of χ for any selected eigenvector is equivalent to detecting all its local features.

2) Local Asymmetry Measurements: As the eigenvectors are isometry-invariant, their topological features are isometry-invariant and intrinsic as well. Hence, they can be used efficiently to quantify the local asymmetries of torso shapes. We define the local asymmetry measures as the differences between the geometric coordinates of the corresponding local features, i.e., local maxima and/or minima on the left (L) and right (R) sides of both the posterior and anterior sides of the torso. Let $P_l = (x_l, y_l, z_l)^T$ and $P_r = (x_r, y_r, z_r)^T$ be the left and right corresponding feature points, respectively. We define, for any pair (P_l, P_r), three asymmetry measures: $A_{\text{offset}} = |x_l| - |x_r|$ is the lateral offset asymmetry, $A_{\text{height}} = |y_l| - |y_r|$ is the height asymmetry, and $A_{\text{depth}} = |z_l| - |z_r|$ is the depth asymmetry. We define the change rate between shapes (pre- versus post-operative) to be the relative difference between their corresponding asymmetries.

III. Experiments and Results

In this section, we focus our experimental analysis on a dataset of patients with AIS recently evaluated by our research group using the cross-sectional based approach [17].

A. Datasets

1) Pre-/Post-Operative Dataset: The dataset consists of adolescent patients with idiopathic scoliosis (AIS) treated at Sainte-Justine Hospital (SJH) in Montreal, Canada. We consider 49 AIS patients (42 female and 7 male), aged 15 ± 2 years, who had a spinal surgery between May 2004 and August 2011 using one of three different surgical techniques. All these patients had the same type of spinal deformation, namely an abnormal spinal curve in the main thoracic region (Lenke 1A curve type [32]). Full torso surfaces were acquired using a non-invasive optical surface digitizing system (InSpeck/Creaform Inc., Lévis, QC). The system provides dense triangulated meshes with 40k to 70k vertices according to the size of patient, with a precision of about 1.1 ± 0.9 (mm) over the surface of the torso [45]. Torso acquisitions were carried out at most 6 months before and 6 months after surgery.

2) Clinical Measurements: The patients also underwent radiographic exams before and after surgery. Several measurements characterizing the spinal deformity are therefore obtained from the radiographic images of the spine. We choose the most important measurements: the Cobb angle (CA) [7], which measures the spinal curvature, and the coronal balance (Cor-Bal) of the spine [13]. In addition to radiographic measurements, the thoracic rib hump was evaluated using a scoliometer manually placed on the back while the patients are in forward-bending posture [46]. Fig. 5 provides descriptive illustrations of these measurements, and Table I reports their statistics before and after surgery. We will use these measurements to evaluate the agreement between the local torso asymmetry changes and the correction rates given by the clinical assessment.

B. Mesh Pre-Processing

The triangulated meshes obtained by the acquisition system are not homogenous over the whole torso shape, with triangles of poor quality in certain areas, notably under the arms (due to occlusion) and in surface regions tangential to the digitizers. The mesh data also contain holes at the boundaries of the trunk, i.e., where the head, arms and pelvis are cropped off, and therefore the graph is not entirely connected. It is, therefore, very important to inspect and enhance the quality of meshes before processing since the Laplacian matrix (Section II-A) is sensitive

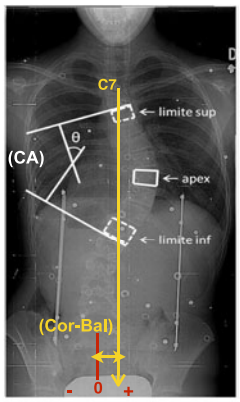

http://www.tsrhc.org/scoliosis-scoliometer

Fig. 5. Visual description of the clinical measurements for scoliosis diagnosis. To the left, a radiographic image of a scoliotic female patient from Saint-Justine hospital. The Cobb angle (CA) is defined as the angle between the lines perpendicular to the upper and lower vertebrae delimiting the main thoracic curve. The coronal balance (Cor-Bal) is defined as the lateral distance between the central sacral vertical line *(in red color)* and the line drawn downwards from the mid-point of the C7 vertebrae *(in yellow color)*. To the right, a web image showing the apical trunk rotation angle (rib hump) at the back measured by the scoliometer.

TABLE I
STATISTICAL DESCRIPTION OF THE CLINICAL MEASUREMENTS ON PRE- AND POST-OPERATIVE TORSO SHAPES

Clinical measurements	Preop	Postop	Relative change (%)
Cobb angle (deg)	58.18 ± 10.37	15.82 ± 6.92	73 ± 33
Rib hump (deg)	12.16 ± 8.60	5.16 ± 5.50	58 ± 36
Cor-Bal (mm)	9.68 ± 19.00	0.23 ± 12.23	98 ± 36

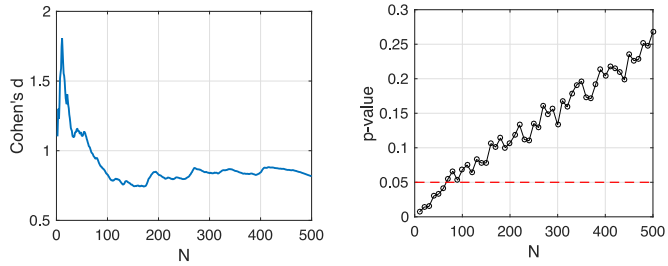

Fig. 6. Spectral feature selection between the two (pre/post-operative) groups of scoliotic torso. To the left, Cohen's d effect size, and to the right, the p-values of the multivariate statistical test of the N-dimensional spectral features between the groups.

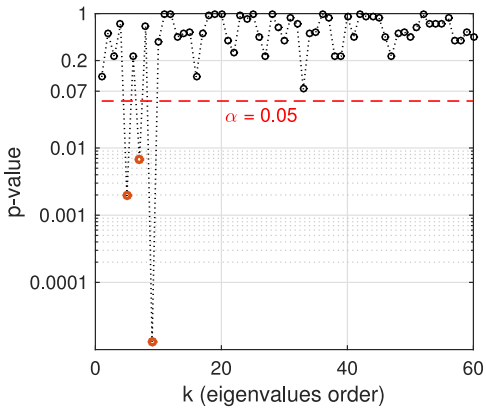

Fig. 7. Multiple comparisons between spectral eigenvalues. The p-values indicate the importance of each of the first 60 eigenvalues. For a test of significance $\alpha \leqslant 5\%$, three eigenvalues (5th, 7th and 9th), highlighted in red, indicate statistically significant differences between pre-/post-operative torso shapes.

to mesh quality. Noise and missing data affect building a stable spectral space of the shape. To solve these issues, we pre-process each trunk mesh using the well-known Radial Basis Functions (RBFs) method [47]. This interpolation technique ensures that a uniform mesh is produced, with high resolution and smooth closing of the surface holes at the trunk boundaries.

C. Spectral Graph Representation and Features Selection

The spectral graph decomposition is applied on the preprocessed mesh data. In all experiments, we fixed the scale factor of the adjacency matrix (1) to the maximum distance between connected nodes, $t = \max_{i,j} \text{dist}(vi, vj)$, in order to give less importance to distant nodes (e.g., nodes at the outliers) while maintaining a relatively smooth representation of the graph. As described in Section II-A, the graph Laplacian is used to define the spectral space of the torso shapes, which is composed of 500 eigenbasis component. The eigenvectors of all samples are rearranged w.r.t an arbitrary reference, i.e., a spectrum chosen from the post-operative subjects. For the statistical analysis, the spectrum is normalized as described in Section II-B.

In order to select the appropriate feature space, we apply the statistical significance (p-value) of the permutation test of the maximum t-statistic and the substantive significance (effect size) of Cohen's d on the eigenvalues between pre-and post-operative subjects (Section II-C1), starting from a vector of $N = 5$ until $N = 500$. Here, the statistical test is sensitive to the difference of at least one eigenvalue, while the effect size is sensitive to the average difference of the entire feature vector. Fig. 6 shows that the p-values of the statistical test increase monotonically when the spectral space dimension increases. The average Cohen's d shows very large effect (>1.20) for $N \leqslant 60$, where the p-values refer to a significant difference $\alpha = 5\%$ between the groups. The average effect size decreases and becomes relatively stable for higher feature vectors ($100 \leqslant N \leqslant 500$). This means that the discrimination power of the spectral feature space is governed by the lower eigenvalues, which are the most important and significant. This is expected, since higher eigenvalues describe high frequency features, which are less related to the changes of torso shape asymmetry.

D. Detection and Identification of the Changes of Local Asymmetries

To study the asymmetry changes between the pre- and post-operative groups of torso shapes, we select the first 60 eigenvalues and apply the multiple comparisons, simultaneously, on the selected components (Section II-C2). Fig. 7 shows the p-values

TABLE II
SIGNIFICANT EIGENVALUES (EVS) OF THE PREOPERATIVE AND POSTOPERATIVE SHAPES REPRESENTED BY THE AVERAGE VALUES

EV	Preop	Postop	Abs-rel change (%)
λ_5	4.7 ± 0.2	4.54 ± 0.17	3.4 ± 15
λ_7	6.53 ± 0.36	6.28 ± 0.32	3.8 ± 11
λ_9	9.66 ± 0.29	9.96 ± 0.25	3.1 ± 14

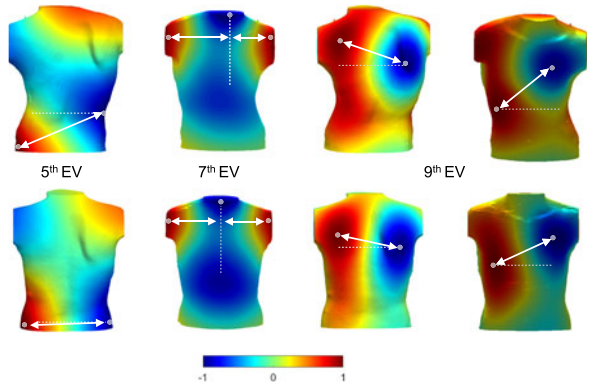

Fig. 8. Illustration of the relevant spectral eigenvector (EV) on a male patient example. The figure shows the *5-th*, *7-th*, and *9-th* eigenvectors of preoperative (top row) and postoperative (bottom row) torso, and the locations of the detected local features (dot points). 1st and 3rd columns show back side; 2nd and 4th columns show front side.

of the FDR-based F-statistic. As can be seen, with a test of significance $\alpha = 5\%$, only 3 out of the 60 eigenvalues change significantly between the pre- and post-operative subjects; they are λ_5, λ_7 and λ_9. Table II provides their average values in each group and the absolute relative change (or difference) between groups.

To identify and quantify the local asymmetries, we use the eigenvectors associated with the three significant eigenvalues. As described in Section II-D, the ECs of upper- (lower-) level sets are computed from each of the *5-th*, *7-th*, and *9-th* eigenvectors. The persistence of the ECs is then determined over the range $[0.5, 1]$, where the maximum persistence is computed and used to indicate the number of connected components and the locations of their corresponding maxima and minima. Consequently, for the *5-th*, *7-th*, and *9-th* eigenvectors, the connected components included one-maxima/one-minima, two-maxima/one-minima, and two-maxima/two-minima, respectively. Fig. 8 illustrates for a sample patient the locations of the local features (maxima and minima) defined by the three eigenvectors on the torso shape. At this stage, we consider the distances between the local features to define the torso left-right (L-R) asymmetries. As can be seen in Fig. 8, the waist height difference (A_{height}) is available from the *5-th* eigenvector. From the *7-th* eigenvector, we compute the difference between the lateral offsets from each shoulder and the base of the neck (A_{offset}). The *9-th* eigenvector represents more local features that allow us to quantify asymmetries at the back and the front, such as the height (A_{height}) and depth (A_{depth}) differences between the shoulder blades and the breast height difference (A_{height}); these

TABLE III
COMPARISON OF THE MEAN LOCAL L-R ASYMMETRIES BETWEEN PRE-OPERATIVE(PREOP) AND POST-OPERATIVE (POSTOP) TRUNKS

Local L-R Asymmetries (mm)	Preop	Postop
Waists Height (WH)	70.30 ± 42.7	48.05 ± 46.5
Shoulder-To-Neck Lat. offsets (STN)	48.78 ± 47.26	22.20 ± 26.06
Shoulder Blades Depth (SBD)	20.18 ± 17.83	17.15 ± 14.90
Shoulder Blades Height (SBH)	93.05 ± 64.76	51.4 ± 48.8
Breasts Height (BH)	99.02 ± 60.33	78.38 ± 58.54

are caused mainly by the rib hump and ribcage rotation. All these measurements can also be expressed in terms of local angles. Table III describes the statistics of the local L-R asymmetries over the whole dataset. Finally, we compute the change rates of the asymmetry measurements between pre- and post-operative shapes in order to evaluate the outcome of surgery.

E. Comparison to the Correction Rates of the Clinical Measurements

We conduct a linear regression analysis to evaluate the agreement between each of the clinical measurements reported in Table I and the change rates of the new asymmetry measurements. Our motivation is to provide an interpretation of the changes captured by the spectral-based shape measurements. This remains challenging since both radiographic and topographic examinations refer to different aspects of scoliosis deformity [48]. Taken $\alpha = 5\%$, significant correlations are found between the CRs in three cases: waist height (WH) asymmetry vs. CA ($\rho = 0.66$, p-value < 0.0001), shoulder-to-neck lateral offset (STN) asymmetry vs. Cor-Bal ($\rho = 0.58$, p-value $= 0.003$), and shoulder-blades depth (SBD) asymmetry vs. scoliometer reading ($\rho = 0.64$, p-value $= 0.0005$).

F. Performance Evaluation of the Spectral Features

In this experiment, we evaluate the robustness of the selected spectral features against irrelevant changes due to the variability of torso shape across the samples. To do so, we performed a comparison between two groups: the first one is composed of 30 postoperative patients whose torso asymmetry (associated with the scoliosis deformity) was significantly reduced after surgery; the second group belongs to a different dataset. It is composed of 30 patients who underwent scoliosis monitoring because of a slight asymmetry of their torso shapes, but they are considered as normal according to the radiographic and clinical examinations. Fig. 9 illustrates, for each eigenvalue, the test of significance obtained by the multiple comparisons between the groups. Taken $\alpha = 5\%$, it can be clearly noticed that the test indicates no significant differences between the shapes as the p-values for all the selected features are higher than 0.1.

IV. DISCUSSION

In this paper, we propose a new framework to analyze pre- to post-operative changes of scoliotic torso shapes based on a

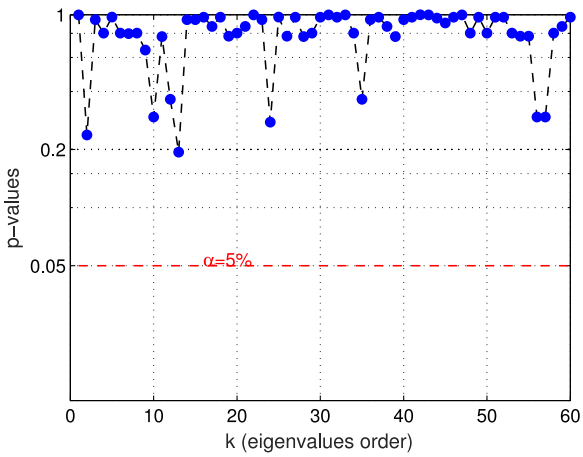

Fig. 9. Performance evaluation of the selected features (first 60 eigenvalues) between groups of normal and postoperative scoliotic torso shapes using multiple comparisons.

spectral representation of geometric torso surface models. Unlike the previous cross-sectional based method [17] that evaluates the global change of torso shape from the back surface rotation (BSR) and trunk lateral shift (TLS), the proposed method benefits from the spectral representation of the torso and uses intrinsic features to compute local shape asymmetries. On the same set of patients, the previous method captured CRs of 18% and 50% for the BSR and TLS, respectively. Our method can evaluate the corrections of *local* trunk surface asymmetries. The differences between shoulder blades indicate CRs of 67% and 64% in height and depth, respectively; the differences between L-R shoulder-to-neck lateral offsets are reduced by 61%; and waist and breast height differences indicate 67% and 52% improvements, respectively. The *5-th* and *7-th* eigenvectors allow us to detect local asymmetries related to the imbalance of the trunk. Interestingly, the *9-th* eigenvector captures asymmetries located at shoulder blades, which are clinically relevant in the visual assessment of scoliosis.

By comparing the pre- to post-operative changes (CRs) between standard clinical measurements and the novel trunk surface asymmetries, our experiments show significant correlations (p–value $< 5\%$) between the coronal balance and the shoulders-to-neck lateral offset, between the scoliometer reading and the shoulder blade depth, and between the thoracic Cobb angle and the waist height, with correlation coefficients $0.5 < \rho < 0.7$. Even though the correlation values are not very strong, the tests of significance (p-values) demonstrate that there is a concordance between spinal (internal) corrections and torso asymmetry (external) corrections. The reproducibility of the local features, as demonstrated by the persistence of the EC of selected eigenvectors, allows for quantifying local shape changes associated with radiographic changes. Other studies [49], [50] attempted to find a relationship between Cobb angles and local asymmetry indices obtained from the surface topography of the back. They reported weak correlations (e.g., $\rho < 0.43$, $p = 0.0001$ between the rib hump and CA [50]) because of the wide error margin of the measurements used and the high variability (in terms of the variance) of the computed shape indices. The moderate correlations they obtained might also have resulted from the fact that surface metrics evaluations did not quantify the same aspects of scoliotic deformation than the internal indices [51]. For instance, the rib hump is only weakly correlated with the CA; the waist height difference, however, is better correlated with the CA ($\rho = 0.66$, $p < 0.0001$).

V. Conclusion

The proposed spectral shape analysis provides a fully automatic approach to detect intrinsic and clinically interpretable local features from the whole scoliotic trunk. Our approach can extract measurements to assess the surgical outcome in terms of correcting shape asymmetry. We analyzed the pre- to post-operative changes in the local asymmetries in a group of patients with main thoracic spinal deformity (Lenke 1A). Although this is a common type of spinal curve, patients with AIS can have other types of spinal deformation. According to [32], they can be classified into 6 different categories. These deformations can be manifested on the surface of the trunk in various ways, making scoliotic torso surface analysis much more challenging in the general case. Future work will focus on including different types of scoliotic deformity. We will, therefore, explore the feasibility of discriminating and comparing scoliotic shapes by their spectral representations. In that context, we notice that the cross-sectional based method developed previously by our team [16], [17] can be combined with the local features proposed here to capture and analyze both global and local shape asymmetries. Another improvement of our method would be to develop a standardized automatic cropping of the torso boundary regions. This process could be achieved, for instance, through a segmentation based on the geometric and textural information provided in the topographic data. So far the boundary cropping process has been done manually and therefore is time-consuming. Finally, once the proposed method is validated on different spinal curve types, our framework could be adopted in scoliosis clinics to help surgeons to better understand the impact of different surgical spinal correction strategies on the torso shape. This could assist the clinician in choosing a surgical approach that will minimize residual trunk asymmetry, for the greater satisfaction of the patient.

Acknowledgment

The authors would like to thank P. Debanné for revising this manuscript and for providing the patient datasets.

References

[1] M. Aebi, "The adult scoliosis," *Eur. Spine J.*, vol. 14, no. 10, pp. 925–948, 2005.
[2] P. Deacon, B. M. Flood, and R. A. Dickson, "Idiopathic scoliosis in three dimensions. A radiographic and morphometric analysis," *J. Bone Joint Surg. Brit.*, vol. 66, no. 4, pp. 509–512, 1984.
[3] L. Hackenberg, E. Hierholzer, W. Pötzl, C. Götze, and U. Liljenqvist, "Rasterstereographic back shape analysis in idiopathic scoliosis after posterior correction and fusion," *Clin. Biomech.*, vol. 18, no. 10, pp. 883–889, 2003.
[4] T. N. Theologis, R. J. Jefferson, A. H. Simpson, A. R. Turner-Smith, and J. C. Fairbank, "Quantifying the cosmetic defect of adolescent idiopathic scoliosis," *Spine*, vol. 18, no. 7, pp. 909–912, 1993.

[5] M. Hawes, "Impact of spine surgery on signs and symptoms of spinal deformity," *Pediatric Rehabil.*, vol. 9, no. 4, pp. 318–339, 2006.

[6] K. Pehrsson, S. Larsson, A. Oden, and A. Nachemson, "Long-term follow-up of patients with untreated scoliosis. A study of mortality, causes of death, and symptoms," *Spine*, vol. 17, no. 9, pp. 1091–1096, 1992.

[7] J. R. Cobb, "Outline for the study of scoliosis," *Amer. Acad. Orthopaedic Surgeons Instructional Course Lectures*, vol. 5, pp. 261–275, 1984.

[8] D. Malfair *et al.*, "Radiographic evaluation of scoliosis: review," *Amer. J. Roentgenol.*, vol. 194, no. 3, pp. S8–S22, 2010.

[9] R. Buchanan, J. G. Birch, A. A. Morton, and R. H. Browne, "Do you see what I see? Looking at scoliosis surgical outcomes through orthopedists' eyes," *Spine*, vol. 28, no. 24, pp. 2700–2704, 2003.

[10] T. Iwahara, M. Imai, and Y. Atsuta, "Quantification of cosmesis for patients affected by adolescent idiopathic scoliosis," *Eur. Spine J.*, vol. 7, no. 1, pp. 12–15, 1998.

[11] V. J. Raso, E. Lou, D. L. Hill, J. K. Mahood, M. J. Moreau, and N. G. Durdle, "Trunk distortion in adolescent idiopathic scoliosis," *J. Pediatric Orthopaedic*, vol. 18, no. 2, pp. 222–226, 1998.

[12] L. E. Amendt, K. L. Ause-Ellias, J. L. Eybers, C. T. Wadsworth, D. H. Nielsen, and S. L. Weinstein, "Validity and reliability testing of the Scoliometer," *Phys. Therapy*, vol. 70, no. 2, pp. 108–117, 1990.

[13] P. O. Newton *et al.*, "Surgical treatment of Lenke 1 main thoracic idiopathic scoliosis: Results of a prospective, multicenter study," *Spine*, vol. 38, no. 4, pp. 328–338, 2013.

[14] P. Patias, T. B. Grivas, A. Kaspiris, C. Aggouris, and E. Drakoutos, "A review of the trunk surface metrics used as scoliosis and other deformities evaluation indices," *Scoliosis*, vol. 5, no. 1, 2010, 12 pp.

[15] P. O. Ajemba, N. G. Durdle, and V. J. Raso, "Characterizing torso shape deformity in scoliosis using structured splines models," *IEEE Trans. Biomed. Eng.*, vol. 56, no. 6, pp. 1652–1662, Jun. 2009.

[16] L. Seoud, J. Dansereau, H. Labelle, and F. Cheriet, "Multilevel analysis of trunk surface measurements for noninvasive assessment of scoliosis deformities," *Spine*, vol. 37, no. 17, pp. E1045–E1053, 2012.

[17] L. Seoud, F. Cheriet, H. Labelle, and S. Parent, "Changes in trunk appearance after scoliosis spinal surgery and their relation to changes in spinal measurements," *Spine Deformity*, vol. 3, no. 6, pp. 595–603, 2015.

[18] M. Styner *et al.*, "Framework for the statistical shape analysis of brain structures using SPHARM-PDM," *Insight J.*, vol. 1071, pp. 242–250, 2006.

[19] D. Nain *et al.*, "Statistical shape analysis of brain structures using spherical wavelets," in *Proc IEEE Int. Symp. Biomed. Imag.*, 2007, vol. 4, pp. 209–212.

[20] L. H. Staib and J. S. Duncan, "Deformable Fourier models for surface finding in 3-D images," *Proc. SPIE*, vol. 1808, pp. 90–104, 1992.

[21] M. Naf, O. Kubler, R. Kikinis, M. E. Shenton, and G. Szekely, "Characterization and recognition of 3d organ shape in medical image analysis using skeletonization," in *Proc. Workshop Math. Methods Biomed. Image Anal.*, 1996, pp. 139–150.

[22] M. Styner, J. A. Lieberman, D. Pantazis, and G. Gerig, "Boundary and medial shape analysis of the hippocampus in schizophrenia," *Med. Image Anal.*, vol. 8, no. 3, pp. 197–203, 2004.

[23] F. R. K. Chung, *Spectral Graph Theory*. Providence, RI, USA: Amer. Math. Soc., 1997.

[24] B. Levy, "Laplace-Beltrami eigenfunctions towards an algorithm that "understands" geometry," in *Proc. IEEE Int. Conf. Shape Model. Appl.*, 2006, pp. 13–20.

[25] H. Zhang, O. Van Kaick, and R. Dyer, "Spectral mesh processing," *Comput. Graph. Forum*, vol. 29, no. 6, pp. 1865–1894, 2010.

[26] M. Reuter, F.-E. Wolter, and N. Peinecke, "Laplace–Beltrami spectra as 'Shape-DNA' of surfaces and solids," *Comput.-Aided Des.*, vol. 38, no. 4, pp. 342–366, 2006.

[27] M. Reuter, F.-E. Wolter, M. Shenton, and M. Niethammer, "Laplace–Beltrami eigenvalues and topological features of eigenfunctions for statistical shape analysis," *Comput. Aided Des.*, vol. 41, no. 10, pp. 739–755, 2009.

[28] A. Qiu, L. Younes, and M. I. Miller, "Intrinsic and extrinsic analysis in computational anatomy," *Neuroimage*, vol. 39, no. 4, pp. 1803–1814, 2008.

[29] J. W. Milnor, *Morse Theory*. Princeton, NJ, USA: Princeton Univ. Press, 1963.

[30] O. Ahmad, H. Lombaert, S. Parent, H. Labelle, J. Dansereau, and F. Cheriet, "Longitudinal scoliotic trunk analysis via spectral representation and statistical analysis," in *MICCAI Workshop on Spectral and Shape Analysis in Medical Imaging* (Lecture Notes in Computer Science), vol. 10126. New York, NY, USA: Springer, 2016, pp. 79–91.

[31] S. Biasotti *et al.*, "Describing shapes by geometrical-topological properties of real functions," *ACM Comput. Surv.*, vol. 40, no. 4, pp. 12:1–12:87, 2008.

[32] L. G. Lenke *et al.*, "Adolescent idiopathic scoliosis: A new classification to determine extent of spinal arthrodesis," *J. Bone Joint Surg. Amer.*, vol. 83-A, no. 8, pp. 1169–1181, 2001.

[33] M. Belkin and P. Niyogi, "Laplacian eigenmaps for dimensionality reduction and data representation," *Neural Comput.*, vol. 15, no. 6, pp. 1373–1396, 2003.

[34] L. J. Grady and J. Polimeni, *Discrete Calculus: Applied Analysis on Graphs for Computational Science*. New York, NY, USA: Springer, Aug. 2010.

[35] M. Reuter, F.-E. Wolter, and N. Peinecke, "Laplace-spectra as fingerprints for shape matching," in *Proceedings of the 2005 ACM Symposium on Solid and Physical Modeling* (SPM '05). New York, NY, USA: Assoc. Comput. Mach., 2005, pp. 101–106.

[36] V. Jain, H. Zhang, and O. Van Kaick, "Non-rigid spectral correspondence of triangle meshes," *Int. J. Shape Model.*, vol. 13, no. 1, pp. 101–124, 2007.

[37] D. Mateus, F. Cuzzolin, R. Horaud, and E. Boyer, "Articulated shape matching by robust alignment of embedded representations," in *Proc. IEEE 11th Int. Conf. Comput. Vis.*, 2007, pp. 1–8.

[38] M. Reuter, "Hierarchical shape segmentation and registration via topological features of Laplace–Beltrami eigenfunctions," *Int. J. Comput. Vis.*, vol. 89, no. 2–3, pp. 287–308, 2009.

[39] H. Lombaert, M. Arcaro, and N. Ayache, "Brain transfer: Spectral analysis of cortical surfaces and functional maps," *Inf. Process. Med. Imag.*, vol. 24, pp. 474–487, 2015.

[40] E. Chung and J. P. Romano, "Multivariate and multiple permutation tests," *J. Econometrics*, vol. 193, no. 1, pp. 76–91, 2016.

[41] J. Cohen, "A power primer," *Psychol. Bull.*, vol. 112, no. 1, pp. 155–159, 1992.

[42] Y. Benjamini and Y. Hochberg, "Controlling the false discovery rate: A practical and powerful approach to multiple testing," *J. Roy. Statist. Soc. B (Methodological)*, vol. 57, no. 1, pp. 289–300, 1995.

[43] O. Ahmad and C. Collet, "Scale-space spatio-temporal random fields: Application to the detection of growing microbial patterns from surface roughness," *Pattern Recognit.*, vol. 58, pp. 27–38, 2016.

[44] D. O. Siegmund and K. J. Worsley, "Testing for a signal with unknown location and scale in a stationary Gaussian random field," *Ann. Statist.*, vol. 23, no. 2, pp. 608–639, 1995.

[45] V. Pazos, F. Cheriet, L. Song, H. Labelle, and J. Dansereau, "Accuracy assessment of human trunk surface 3d reconstructions from an optical digitising system," *Med. Biol. Eng. Comput.*, vol. 43, no. 1, pp. 11–15, 2005.

[46] N. D. Scutt, P. H. Dangerfield, and J. C. Dorgan, "The relationship between surface and radiological deformity in adolescent idiopathic scoliosis: effect of change in body position," *Eur. Spine J.*, vol. 5, no. 2, pp. 85–90, 1996.

[47] J. C. Carr *et al.*, "Reconstruction and representation of 3d objects with radial basis functions," in *Proceedings of the 28th Annual Conference on Computer Graphics and Interactive Techniques* (SIGGRAPH '01). New York, NY, USA: Assoc. Comput. Mach., 2001, pp. 67–76.

[48] L. Seoud, J. Dansereau, H. Labelle, and F. Cheriet, "Noninvasive clinical assessment of trunk deformities associated with scoliosis," *IEEE J. Biomed. Health Informat.*, vol. 17, no. 2, pp. 392–401, Mar. 2013.

[49] I. A. Stokes and M. S. Moreland, "Concordance of back surface asymmetry and spine shape in idiopathic scoliosis," *Spine*, vol. 14, no. 1, pp. 73–78, 1989.

[50] N. Suzuki, K. Inami, T. Ono, K. Kohno, and M. Asher, "Analysis of posterior trunk symmetry index (POTSI) in scoliosis. Part 1," in *Research Into Spinal Deformities 2* (Studies in Health Technology and Informatics), vol. 59. Amsterdam, The Netherlands: IOS Press, 1999, vol. 59, pp. 81–84.

[51] C. J. Goldberg, M. Kaliszer, D. P. Moore, E. E. Fogarty, and F. E. Dowling, "Surface topography, Cobb angles, and cosmetic change in scoliosis," *Spine*, vol. 26, no. 4, pp. 55–63, 2001.